2-1. アミノ酸誘導体（Fig. 1）

腫瘍細胞では増殖に必要なタンパク合成が盛んであり、原料であるアミノ酸を輸送するアミノ酸トランスポーターが細胞膜に高発現している。そこで、この発現量の変化を細胞増殖能の指標とし、さらに生体内での安定性を考慮した人工アミノ酸を分子プローブとして活用する試みがなされている。

α-メチル-L-タイロシンの芳香環3位に ^{18}F を導入した化合物、[^{18}F]FAMT は[^{18}F]FDG と比較して腎臓以外の主要組織、すなわち脳、心臓、肝臓等における生理的集積の低下を認め、脳腫瘍を明瞭に画像化できることが報告された[1]。また、L-タイロシン芳香環の 4 位の水酸基を O-[^{18}F]フルオロエチル化した[^{18}F]FET も炎症組織には集積しないことから、腫瘍との鑑別診断が可能であり、さらに、脳腫瘍の悪性度診断を目標としたプローブとしても臨床評価が進められている[2]。一方、アミノ酸α炭素を含む環状構造を側鎖に有するα-アミノシクロブタン-1-カルボン酸（ACBC）に ^{18}F を導入した PET プローブ、anti-[^{18}F]FACBC を用いることにより、FDG-PET では特定が困難な前立腺癌の描出にも成功している[3]。

2-2. ヌクレオシド誘導体（Fig. 2）

アミノ酸と同様、腫瘍における代謝機能亢進の測定を目的としたプローブとして、ヌクレオシド誘導体が開発されている。DNA 合成能の評価は、^{3}H 標識核酸誘導体を用いることで、生化学分野において基礎的に検討されたが、PET プローブでは、その使用目的を考慮し、インビボでの安定性と動態の改善を目指した分子設計が進められてきた。

3′-デオキシ-3′-^{18}F-フルオロチミジン（[^{18}F]FLT）はピリミジントランスポーターを介して細胞に取り込まれ、細胞質に存在するチミジンキナーゼ（TK_1）により 5′位の水酸基がリン酸化を受けることで捕捉される、いわゆるメタボリックトラッピング型プローブである。すなわち、その集積は細胞の TK_1 活性を反映し、DNA 合成能（細胞増殖能）を間接的に評価できる（Fig. 3）。[^{18}F]FLT は肝臓への高い非特異的集積と骨髄への生理的集積を示すが、正常脳への分布が低いことから、特に脳腫瘍の診断に有効である（Fig. 4）。

一方、抗癌剤や放射線照射による治療で、DNA 合成は抑制されているものの、TK_1 活性が維持された状態では、[^{18}F]FLT の集積は腫瘍の増殖能を反映しない。この問題を解決する目的で、TK_1 基質選択性、DNA 取込み能、動態解析に適した体内挙動を有するプローブの開発が試みられた。近年報告された 4′-^{11}C-メチルチオチミジン（[methyl-^{11}C]*S*-dThd）は増殖組織への選択的集積を示し、さらに DNA 合成能と高く相関していたことから、新たな核酸代謝イメージングプローブとして期待されている[4]。

2-3. 低酸素領域イメージングプローブ（Fig. 5）

腫瘍組織内には、活発な細胞増殖の過程で、栄養血管からの酸素供給が不十分となった領域が存在することが明らかとなっている。これら低酸素領域の腫瘍は

一般的に抗癌剤や放射線に対する感受性が低いことから、腫瘍組織の低酸素状態を把握することは、化学療法や放射線治療の計画を立てる上で非常に有効であると考えられる。

低酸素細胞の増感剤の構造をもとに設計、開発された、2-ニトロイミダゾール骨格を有する ^{18}F-フルオロミソニダゾール（[^{18}F]FMISO）は、酸素分圧が数 mmHg まで低下した低酸素環境下では、分子内のニトロ基がラジカルあるいはアミンに還元され、細胞内成分と結合することにより滞留するモデルが考えられている（Fig. 6）。本プローブは、その脂溶性の高さに起因する血液クリアランスの遅延が画像を撮像する際の問題となっており、脂溶性を低減させる分子設計がなされた。現在、臨床での利用が試みられているプローブとして、同じく 2-ニトロイミダゾール誘導体の PR-170 を ^{18}F 標識した[^{18}F]FRP-170 があり、画像コントラストの改善と、投与後から撮像までに要する時間の短縮が達成されている[5]（Fig. 7）。

また、近年では放射性銅を用いたキレート化合物の Cu-ATSM も注目されている。脂溶性低分子錯体の Cu-ATSM は生体膜を容易に透過するため、正常組織では滞留性を示さない。しかし、低酸素組織ではミクロソーム電子伝達系の酵素により 2 価の銅が 1 価に還元され、ATSM との結合から遊離した Cu^{+}が細胞内に滞留する（Fig. 8）。複数存在する銅の放射性同位体の中で、半減期 9.7 分の ^{62}Cu はジェネレーターにて産生されることから、汎用性の高い診断への利用が期待できる[6]。本邦では放射線医学総合研究所で製造した ^{62}Zn-^{62}Cu ジェネレーターを複数の PET 施設に供給し、ATSM キット化製剤を用いて ^{62}Cu-ATSM を調製、臨床使用する計画も進行中である。一方、^{64}Cu は半減期が 12.7 時間であるため、^{64}Cu-ATSM を用いた場合は、腫瘍低酸素状態の時間的／空間的変化を長時間追跡することが可能となり、より詳細な病態解明に繋がると考えられる。

2-4. アポトーシスイメージングプローブ

アポトーシスは DNA 損傷を受けた、あるいは体内で不要となった細胞が自らを排除するためにプログラム化された細胞死の様式であるが、抗癌剤や放射線治療に対する腫瘍細胞の感受性は、アポトーシスの誘発と関連することが報告されている。したがって、アポトーシスイメージングは腫瘍を治療するにあたり、薬物や照射放射線の用量を決定するための意義が大きい。

アポトーシスを描出する PET プローブとしては、^{18}F もしくは ^{124}I で標識したアネキシン A5 が検討されている。アネキシン A5 は分子量 36 kDa のタンパクであり、正常細胞では細胞膜内側に存在するホスファチジルセリンがアポトーシス細胞膜に表出した際、これと選択的に結合する（Fig. 9）。基礎実験では、^{18}F 標識体を用い、シクロヘキシミドでアポトーシスを誘導したラットの肝臓へのプローブの集積が確認された[7]。また、アポトーシスは虚血性疾患や神経変性疾患にも関連しており、これら病態のイメージングも試みられている。

2-5. 浸潤・転移に関わるタンパクを標的としたイメージングプローブ

腫瘍の悪性度を診断するため、分子生物学的な知見に基づき、腫瘍組織あるいは細胞で特異的に発現する遺伝子、タンパク情報を可視化するプローブの開発も精力的に進められている。

例えば、腫瘍細胞周囲のマトリックス分解酵素であるマトリックスメタロプロテイネース（MMP）や血管新生に関与するインテグリンαVβ3は、腫瘍細胞が浸潤、転移する際に発現の亢進を認めることから、それぞれに結合するプローブとして^{18}F-SAVO3や^{18}F-RGDペプチドが開発されている[8, 9]。

また、上皮成長因子受容体に類似した構造を有するHer-2の発現や活性化は細胞の異常増殖性に深く関与しており、近年ではトラスツズマブ等のHer-2阻害薬が治療に使用されるようになった。しかし、特定の分子を阻害する薬物を用いる治療設計では、当該分子が異常発現あるいは活性化している場合においてのみ効果が期待されるため、必然的に有効な患者群は限定される。したがって、受容体を定量評価することで治療効果の予測が可能となれば、効率的な治療と患者の負担軽減を実現できる。以上を背景として、Her-2を認識する抗体性分子に^{18}Fを導入した[^{18}F]FBEM-$Z_{HER2:342}$が開発され、本プローブは、担癌ヌードマウスを用いた検討において良好な腫瘍集積性を示した[10]。今後、同様の概念を臨床展開するためには体内動態の改善が必要であり、低分子化を含めた分子設計と同時に新規化合物の探索が望まれる。

3. 心血管系イメージングプローブ

核医学診断法による心機能の評価として、現在の臨床で実施されている試験は、ほとんどが心筋血流量と組織壊死の判定に関するものに限られている。しかし、近年では分子生物学の発展に伴い、エネルギー代謝や交感／副交感神経支配による機能制御機構と種々の疾患との関連、および病態に関与する分子の存在が明らかとなってきた。このため、今後は心臓に発現するタンパクを標的とした定量解析が潮流の一つに加わり、新規プローブを用いた、非虚血性心疾患の超早期画像診断が加速すると期待される。また、動脈硬化病変に存在する血栓のイメージングも、生活習慣病罹患者数が急増している状況を踏まえ、予防核医学的診断としての重要性が増すと考えられる。

3-1. 心筋血流量イメージングプローブ

心筋血流の検査は、しばしば緊急性を求められることから、ジェネレーター産生核種によるPET検査の拡大が期待される。今後、本邦でジェネレーターの供給体制が整えば、前述の^{62}Cuによる^{62}Cu-PTSM（脳／心筋血流量測定プローブ）[6]（Fig. 10）や^{82}Sr-^{82}Rbジェネレーターから溶出される^{82}Rb^{+}[11]（K^{+}と類似の挙動を取る）を用いた臨床診断が可能となる。特に後者は半減期が1.3分と非常に短いため、同日複数回検査にも対応できる。

3-2. NETイメージングプローブ

心臓は交感神経と副交感神経による拮抗的二重支配を受けているが、心室筋は交感神経による単独支配であり、治療薬には交感神経系を標的とするものが多い。一方、画像診断においても、交感神経終末に存在するノルエピネフリントランスポーター（NET）発現量の減少と、虚血性心疾患や心不全等の病態との関連が注目されている。そこで、MIBG等、従来のNET基質として細胞内に輸送されるタイプとは異なるNET結合型プローブとして、NET選択的阻害薬であるレボキセチンを母体とする放射性ヨウ素標識(*S, S*)-IPBMが報告されたが[12]（Fig. 11）、^{18}F, ^{76}Br, ^{124}I等のハロゲンPET核種で標識した類似のプローブにより、新たな臨床心機能評価が実現する可能性がある。

3-3. 動脈硬化病変イメージングプローブ

予防医学的見地から、脳卒中や心筋梗塞に代表される動脈狭窄病変が発症する以前に、動脈内皮の機能障害あるいは不安定プラークを検出することが極めて重要であり、PETによる高精度の診断が求められている。血栓形成過程は活性型マクロファージの浸潤と泡沫化、細胞の炎症性応答、これに伴う各種バイオマーカーの出現として特徴づけられるが、以上の現象は、細胞間質の分解や血管新生、アポトーシス細胞の出現等、多くの生化学的、分子生物学的変化を伴う。

現在、臨床では[^{18}F]FDGがマクロファージに集積することを利用したプラークの検出が一定の成果を上げているが、今後はさらに、lectin-like oxidized LDL receptor-1（LOX-1）[13]を始めとするスカベンジャー受容体や、マトリックスメタロプロテイネース（MMP）等を新たな標的分子とし、脂質代謝や機能性タンパクの定量により、プラーク形成のステージを評価するプローブの開発が期待される。

4. 脳イメージングプローブ

脳のイメージングには、その目的に応じて形態画像、機能画像が用いられるが、精神神経疾患の診断や治療への展開を考えた場合、受容体やトランスポーター密度、神経伝達物質の生合成や代謝に関する神経機能の評価が重要となる。さらに、Aβプラーク（老人斑）や過剰リン酸化タウタンパクの細胞内蓄積（神経原線維変化）等、脳内に特異的に発現した分子を標的とした、神経変性疾患の早期診断が注目されている。

脳機能を描出するプローブには、本稿の最初に記載した条件に加え、血液脳関門の高い透過性が要求される。したがって、化合物の脂溶性や電荷、分子量を総合的に考慮した分子設計が必要であり、基本的には低分子化合物を母体としてプローブの最適化が行われる。

4-1. 機能性タンパクのイメージングプローブ（Fig. 12）

受容体やトランスポーター、酵素等の機能性タンパクを標的としたイメージングプローブの開発は古くから進められており、主として神経変性疾患における病態や治療薬の作用機序、動態の解明に活用されてきた。現在ではこれらに加え、疾患の鑑別診断の手段として、特定のタ

ンパク発現をサブタイプレベルで可視化する分子プローブが用いられている。

アセチルコリン神経系は認知機能障害に関与し、特にα4β2ニコチン性アセチルコリン受容体の画像化が重要視されてきた。近年では、同受容体に対して高い親和性を有するエピバチジン誘導体の中で[^{18}F]2-F-A-85380の臨床評価が進められ、アルツハイマー型認知症（AD）患者において集積の有意な減少と、病気の進行度との相関性が報告された[14]。

また、臨床症状が類似しているADとレビー小体型認知症（DLB）との鑑別には、しばしばドパミン神経系の評価が有効となる。シナプス前神経終末に存在する小胞モノアミントランスポーター（VMAT2）を標的とした ^{11}C-(+)-α-ジヒドロテトラベナジン（[^{11}C]DTBZ）を用いた検討では、本プローブの線条体への集積は、DLB患者においてAD患者よりも低くなることが報告されている[15]。

4-2. Aβプラーク／神経原線維変化イメージングプローブ

現在のAD診断では、いわゆるアミロイド仮説に基づき、老人斑の構成成分であるAβプラークの定量的イメージングが注目されている。ベンゾチアゾール誘導体の[^{11}C]PIBは、PET撮像が2002年に初めてヒトで施行されて以降、欧米で大規模な臨床評価が行われてきた。その結果、本プローブは、健常者と比較してAD患者の大脳皮質および線条体に高く集積することが明らかとなった[16]（Fig. 13）。さらに[^{11}C]PIBの脳集積が高かった軽度認知障害（MCI）患者は高い確率でADへと移行することが示されており、認知機能障害の予後予測を実現するプローブとして、治療方針決定への応用が期待されている[17]。

また、近年では、Aβプラークよりも神経原線維変化の脳内蓄積の方がADの進行度と相関性が高いことも示唆されており、後者（過剰リン酸化タウタンパク）を標的としたPETプローブの開発も行われている。現時点では、Aβプラークと過剰リン酸化タウタンパクとの間に結合交差性を有する（双方に結合する）プローブも多いが、今後、凝集体の三次元構造に関してさらなる情報が得られれば、これがプローブの分子設計にも反映されると考えられる。

5. おわりに

以上、現在注目されているPETプローブを「post-FDGプローブ」として幾つか紹介したが、これら以外にも糖尿病や遺伝子治療におけるレポーター遺伝子等、画像化の標的は臨床／研究のニーズに応じて数多く存在しており、それぞれに対応したプローブが精力的に開発されている。今後、本邦でもこれらのプローブを用いた臨床データが纏められ、高い評価が得られれば、普遍的なPET薬剤として使用されるようになる可能性がある。さらに、自動合成装置の進歩とともに高速*C*-^{11}Cメチル化や効率的な^{18}Fフッ素化反応に関する研究も進んだことから、分子内での放射性核種の導入位置に関し、ある程度高い自由度を持ってプローブを合成することが可能となった。今後、標的分子の研究と、合成技術の発展との相乗

効果により、多岐に渡る疾患や生命現象を包含し得るPET薬剤開発の発展と革新的イメージングの実現を期待したい。

文献

1) Inoue T et al : The Journal of Nuclear Medicine **40** : 399-405, 1999
2) Floeth FW et al : The Journal of Nuclear Medicine **49** : 730-737, 2008
3) Schuster DM et al : The Journal of Nuclear Medicine **48** : 56-63, 2007
4) Toyohara J et al : Nuclear Medicine and Biology **35** : 67-74, 2008
5) Kaneta T et al : Annals of Nuclear Medicine **21** : 101-107, 2007
6) Wong TZ et al : American Journal of Roentgenology **192** : 427-432, 2008
7) Yagle KJ et al : The Journal of Nuclear Medicine **46** : 658-666, 2005
8) Furumoto S et al : Nuclear Medicine and Biology **30** : 119-125, 2003
9) Kenny LM et al : The Journal of Nuclear Medicine **49** : 879-886, 2008
10) Kramer-Marek G et al : European Journal of Nuclear Medicine and Molecular Imaging **35** : 1008-1018, 2008
11) Manabe O et al : The Journal of Nuclear Medicine **50** : 68-71, 2009
12) Kiyono Y et al : Nuclear Medicine and Biology **35** : 213-218, 2008
13) Ishino S et al : The Journal of Nuclear Medicine **49** : 1677-1685, 2008
14) Sabri O et al : European Journal of Nuclear Medicine and Molecular Imaging **35** : S30-45, 2008
15) Gilman S et al : Annals of Neurology **55** : 774-780, 2004
16) Klunk WE et al : Annals of Neurology **55** : 306-319, 2004
17) Forsberg A et al : Neurobiology of Aging **29** : 1456-1465, 2008

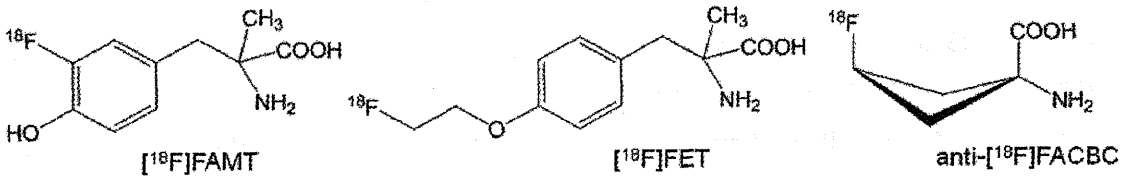

Figure 1　アミノ酸誘導体型腫瘍イメージング分子プローブ

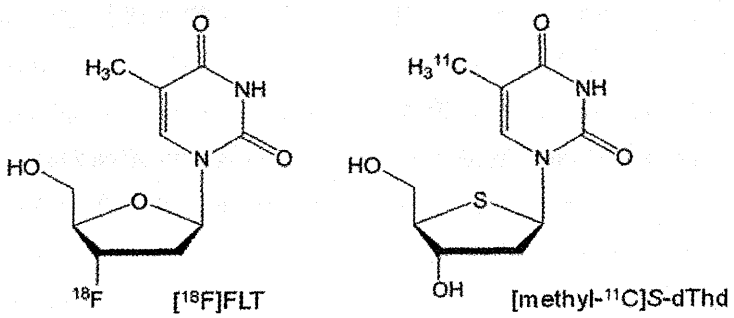

Figure 2　ヌクレオシド誘導体型腫瘍イメージング分子プローブ

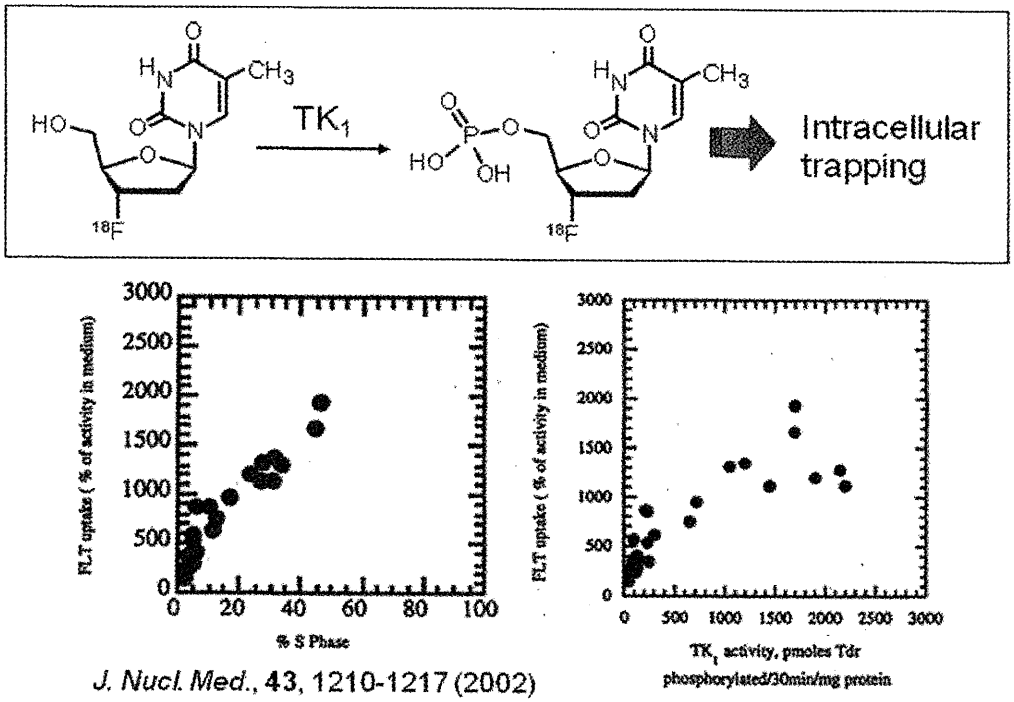

※ 左： DNA 合成期（S 期）にある腫瘍細胞の存在率（横軸）と FLT 取込み量（縦軸）の関係，右： 腫瘍細胞の TK_1 活性（横軸）と FLT 取込み量（縦軸）の関係
細胞増殖期にある（TK_1 活性が高く DNA 合成が盛んな）細胞へは、[^{18}F]FLT が高く取り込まれることを示唆している。

Figure 3　細胞増殖能を標的とした[^{18}F]FLT による腫瘍イメージング

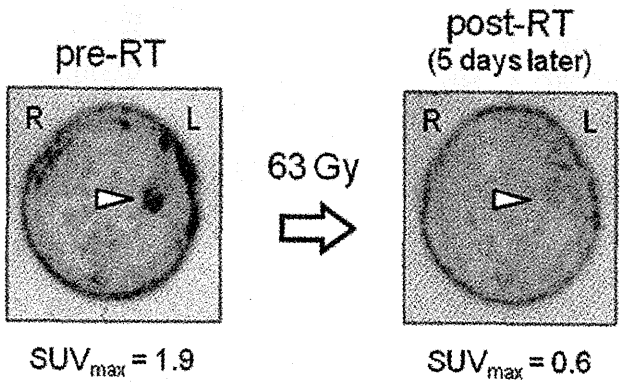

※ Glioblastoma 手術後残存腫瘍に対する放射線治療の治療効果判定。治療の前後で[^{18}F]FLT-PET を施行した結果、放射線治療終了 5 日後で、腫瘍への集積は顕著に低下した。治療前に認められる左側頭部表面の集積は、手術後の創部への集積を示すものと考えられる。

Figure 4　[^{18}F]FLT による放射線照射の治療効果判定

TOPIX post-FDG：放射性薬剤の未来

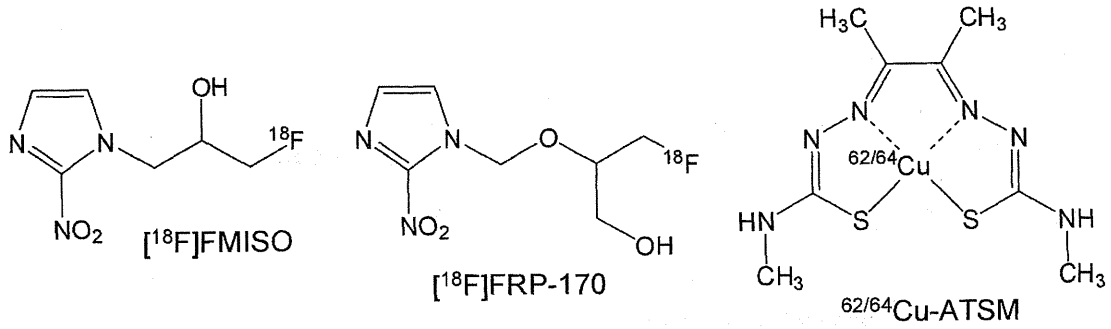

Figure 5　低酸素組織イメージングプローブ

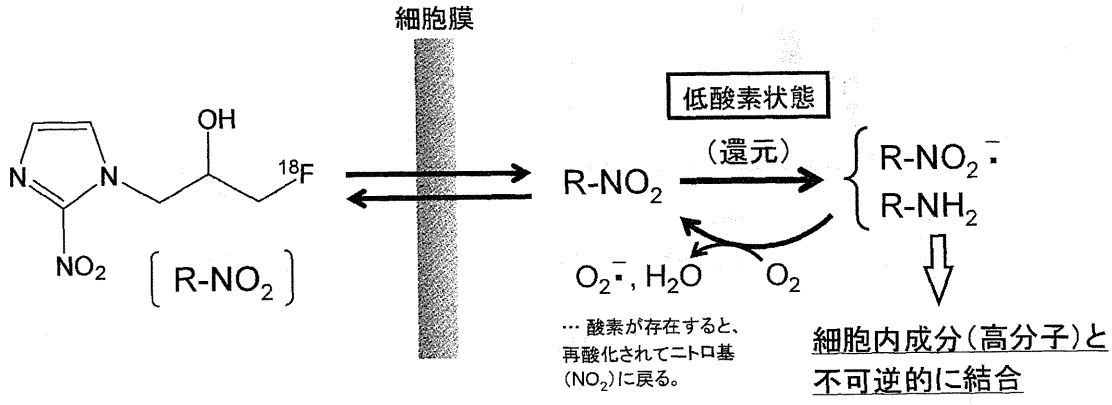

Figure 6　[18F]FMISOの低酸素細胞への集積機序

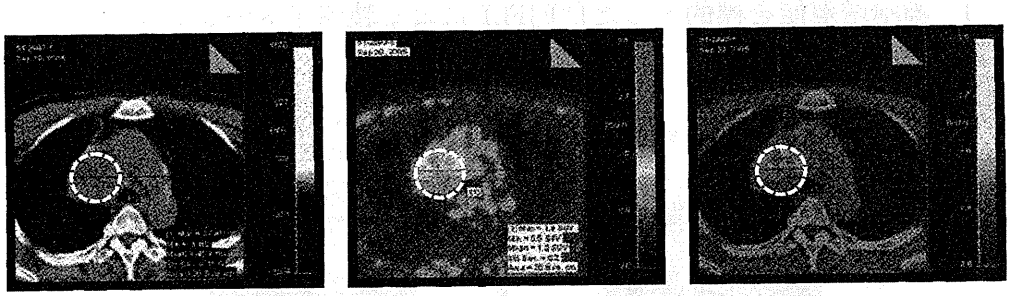

J. Am. Geriatr. Soc., ***55***, 1142-1144 (2007)

※ cT2N3M0, Stage IIIBの肺腺癌患者(最大腫瘍径:65 mm)を[18F]FRP-170にて描出した結果(破線内)。SUV_{max} = 2.0であった。

Figure 7　[18F]FRP-170による肺腺癌のイメージング

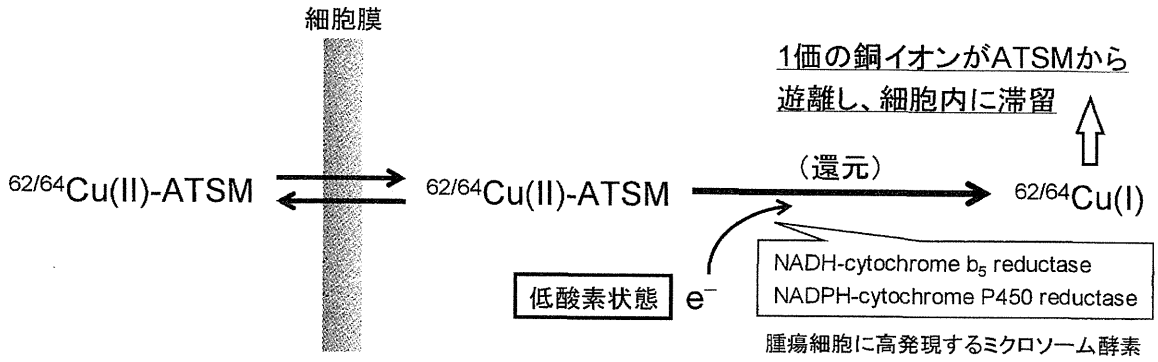

Figure 8　$^{62/64}$Cu-ATSM の低酸素細胞への集積機序

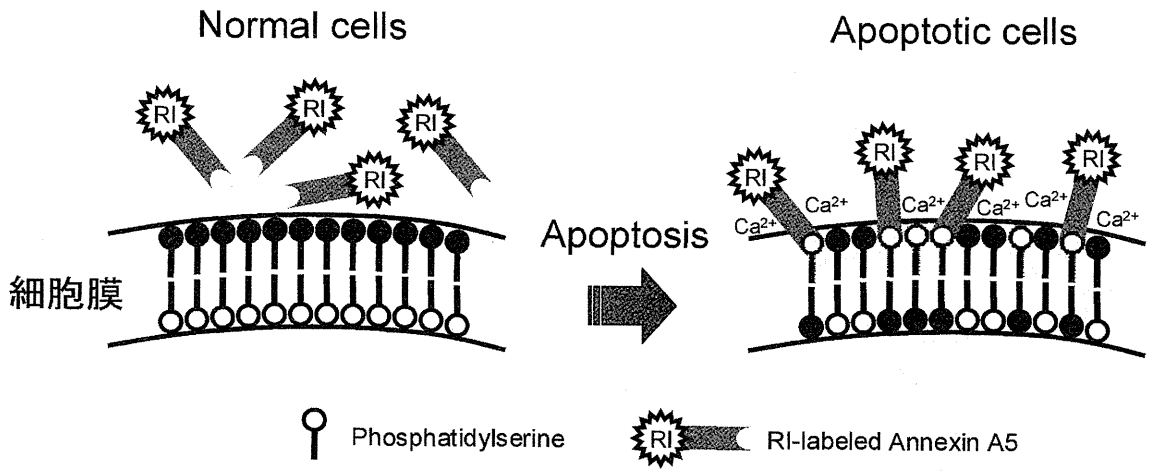

Figure 9　放射性核種標識 Annexin A5 のアポトーシス細胞膜への集積機序

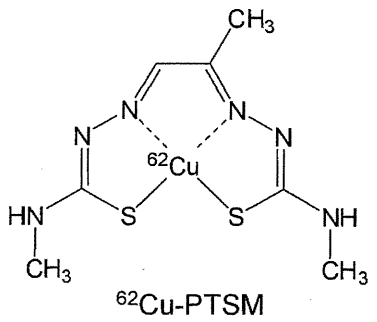

Figure 10　心筋血流量イメージングプローブ

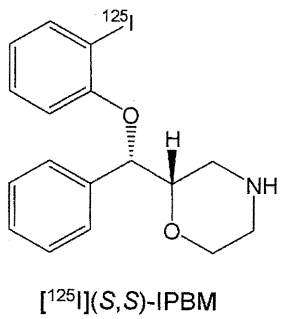

Figure 11　NET イメージングプローブ

TOPIX post-FDG：放射性薬剤の未来

α4β2ニコチン性アセチルコリン受容体イメージングプローブ

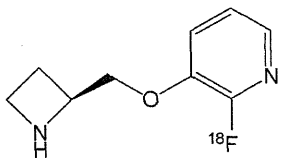

[18F]2-F-A-83580

シナプス小胞モノアミントランスポーターイメージングプローブ

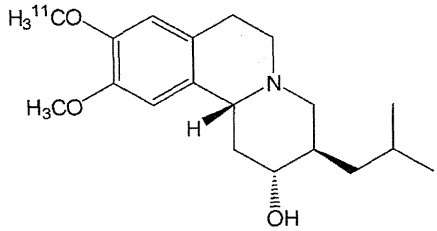

(+)-[11C]DTBZ

Figure 12　脳に発現する機能性タンパクのイメージングプローブ

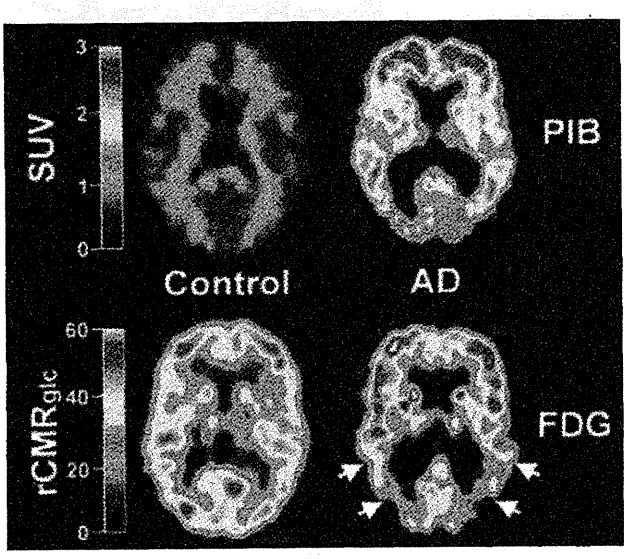

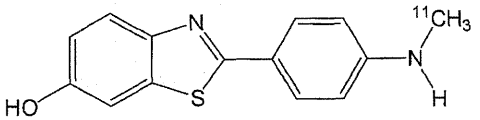

[11C]PIB

※ アルツハイマー型認知症患者(AD)脳における、[11C]PIBと[18F]FDGの集積。老年健常者(Control)と比較し、[11C]PIBは前頭葉および頭頂側頭葉に高く集積した。[18F]FDGは頭頂側頭葉に典型的な糖代謝の低下を認めた(矢印)。

Ann. Neurol., ***55***, 306-319 (2004)

Figure 13　[11C]PIB による脳内 Aβプラークのイメージング

Bioorganic & Medicinal Chemistry Letters 20 (2010) 3885–3888

Contents lists available at ScienceDirect

Bioorganic & Medicinal Chemistry Letters

journal homepage: www.elsevier.com/locate/bmcl

Development of dual functional SPECT/fluorescent probes for imaging cerebral β-amyloid plaques

Masahiro Ono [a,*], Manami Ishikawa [a], Hiroyuki Kimura [a], Shun Hayashi [a], Kenji Matsumura [a], Hiroyuki Watanabe [a], Yoichi Shimizu [a], Yan Cheng [a], Mengchao Cui [a], Hidekazu Kawashima [b], Hideo Saji [a,*]

[a] Graduate School of Pharmaceutical Sciences, Kyoto University, 46-29 Yoshida Shimoadachi-cho, Sakyo-ku, Kyoto 606-8501, Japan
[b] Graduate School of Medicine, Kyoto University, Shogoin Kawahara-cho, Kyoto 606-8507, Japan

ARTICLE INFO

Article history:
Received 20 April 2010
Revised 7 May 2010
Accepted 11 May 2010
Available online 16 May 2010

Keywords:
Alzheimer's disease
β-Amyloid plaque
Positron emission tomography
Single photon emission computed tomography
Fluorescence
Dual imaging

ABSTRACT

The imaging of β-amyloid (Aβ) aggregates in the brain may lead to the early detection of Alzheimer's disease (AD) and monitoring of the progression and effectiveness of treatment. The purpose of this study was to develop dual modality SPECT and fluorescent probes based on boron dipyrromethane (BODIPY) as a core structure. We designed and synthesized an ^{125}I-labeled derivative of BODIPY (BODIPY7). BODIPY7 had a K_i value of 108 nM for Aβ(1–42) aggregates and exhibited peaks of absorption/emission at 606/613 nm. It detected Aβ plaques in sections of brain tissue from an animal model of AD and displayed low uptake in the brain and high uptake in the liver in normal mice. Although additional modifications of the BODIPY scaffold are necessary to improve brain uptake, these results should aid the development of dual functional SPECT/fluorescent probes for the imaging of Aβ plaques in the brain.

The formation of β-amyloid (Aβ) plaques is a key neurodegenerative event in Alzheimer's disease (AD).[1,2] Since the imaging of these plaques in vivo may lead to the presymptomatic diagnosis of AD, many molecular probes, including positron emission tomography (PET)[3–6] and single photon emission computed tomography (SPECT)[7,8] tracers labeled with a radioisotope (RI), have been developed. The PET ligand [^{11}C]-2-(4-(methylamino)phenyl)-6-hydroxybenzothiazole (PIB) with a benzothiazole backbone has shown particular promise in early clinical trials and is currently being used in a number of human studies.[9,10] Nuclear imaging with PET/SPECT probes is an established clinical modality that offers good sensitivity deep in tissue, which permits whole body quantitative imaging not only in small animals but also in humans. However, it is limited by factors such as a time-consuming data acquisition process, expensive equipment, exposure to radioactivity, the need for highly skilled personnel, and a relatively poor spatial resolution.[11]

In addition to PET/SPECT probes, much attention has focused on the development of near-infrared fluorescent (NIRF) probes targeting Aβ plaques.[12–14] Optical imaging with NIRF probes is a relatively new modality that offers real-time, nonradioactive, and, depending on the technique, high-resolution imaging. Among NIRF probes reported to date, NIAD-4[13] and CRANAD-2[15] cross the blood–brain barrier, selectively bind Aβ with high affinity, clear quickly from the brain, and absorb and emit within the near-infrared region (650–900 nm), often called the 'optical window'.[16] Optical imaging techniques are not quantitative, especially when the object is located deep to the skin because of significant signal attenuation in tissue, but NIRF imaging has the potential to provide a rapid, inexpensive, and nonradioactive drug screening system for AD.

Currently, in vivo imaging of Aβ plaques in AD brains is primarily performed using nuclear imaging techniques such as SPECT and PET. We hypothesize that the development of dual functional nuclear/fluorescent imaging probes not only can provide complementary information that may lead to improve diagnosis and management of AD patients, but also can facilitate the validation of optical imaging by standard nuclear imaging techniques. Although several recent papers demonstrate the usefulness of dual nuclear and fluorescent imaging probes targeting tumor,[17,18] such dual functional probes for Aβ plaques have not been reported. Here, we propose a design strategy for the development of a dual SPECT/fluorescent probe for Aβ plaques in the brain. In this study, we selected boron dipyrromethane (BODIPY), one of the most useful fluorophores,[19–23] and introduced the radiolabeled moiety

* Corresponding authors. Tel.: +81 75 753 4608; fax: +81 75 753 4568 (M.O.); tel.: +81 75 753 4556; fax: +81 75 753 4568 (H.S.).
E-mail addresses: ono@pharm.kyoto-u.ac.jp (M. Ono), hsaji@pharm.kyoto-u.ac.jp (H. Saji).

0960-894X/$ - see front matter © 2010 Elsevier Ltd. All rights reserved.
doi:10.1016/j.bmcl.2010.05.027

NIAD-4, 2-(4-[^{125}I]iodophenyl)-5-thiophene, at the 3-position. Described herein is the synthesis and characterization of this radioiodinated derivative of BODIPY. To our knowledge, this is the first time dual SPECT/fluorescent probes have been proposed as probes for imaging Aβ plaques in the brain.

The target BODIPY derivative was prepared as shown in Scheme 1. The compound **1** was synthesized in a yield of 21.4% by the Suzuki coupling reaction. After reduction of the aldehyde to an alcohol by $NaBH_4$, the desired Wittig reagent **3** was readily prepared from **2** and triphenylphosphine. The compound **3** was produced by a Wittig reaction between **3** and pyrroaldehyde. The key step in the formation of the BODIPY backbone was accomplished by the condensation of pyrrole-2-carboxylaldehyde and **4** at low temperature, followed by the addition of $BF_3{\cdot}OEt_2$. The bromo compound (**5**) was reacted with bis(tributyltin) using Pd(0) as a catalyst, and the corresponding tributyltin derivative (**6**) was obtained in a yield of 17.0%. The tributyltin derivative (**6**) was readily reacted with iodine in chloroform at room temperature to give the iodo derivative (**7**) in a yield of 20.0%. The radioiodination was achieved by the same iododestannylation reaction using hydrogen peroxide as the oxidant, which produced the desired radioiodinated ligand, [^{125}I]BODIPY7, in a yield of 25% and with greater than 95% radiochemical purity. It is anticipated that the no-carrier-added preparation resulted in the final product bearing similar theoretical specific activity to ^{125}I.

To quantify the affinity of BODIPY7 for Aβ plaques, we carried out inhibition assays on the binding to Aβ(1–42) aggregates with

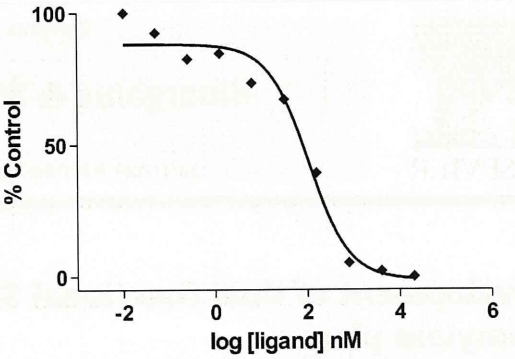

Figure 1. Curve of BODIPY7's inhibition of the binding of [^{125}I]IMPY to Aβ(1–42) aggregates.

[^{125}I]IMPY as a competing radioligand. BODIPY7 inhibited the binding of [^{125}I]IMPY in a dose-dependent manner, indicating that it has affinity for Aβ(1–42) aggregates (Fig. 1). This result suggests that the binding sites of BODIPY7 and IMPY partly overlap. BODIPY7 had a K_i value of 108 nM, indicating sufficiently high affinity for Aβ aggregates. A recent paper reported that the introduction of the triazole moiety into the BODIPY scaffold afforded dyes that allowed for the unambiguous differentiation of an unordered conformation, which is mostly a benign form, from an ordered

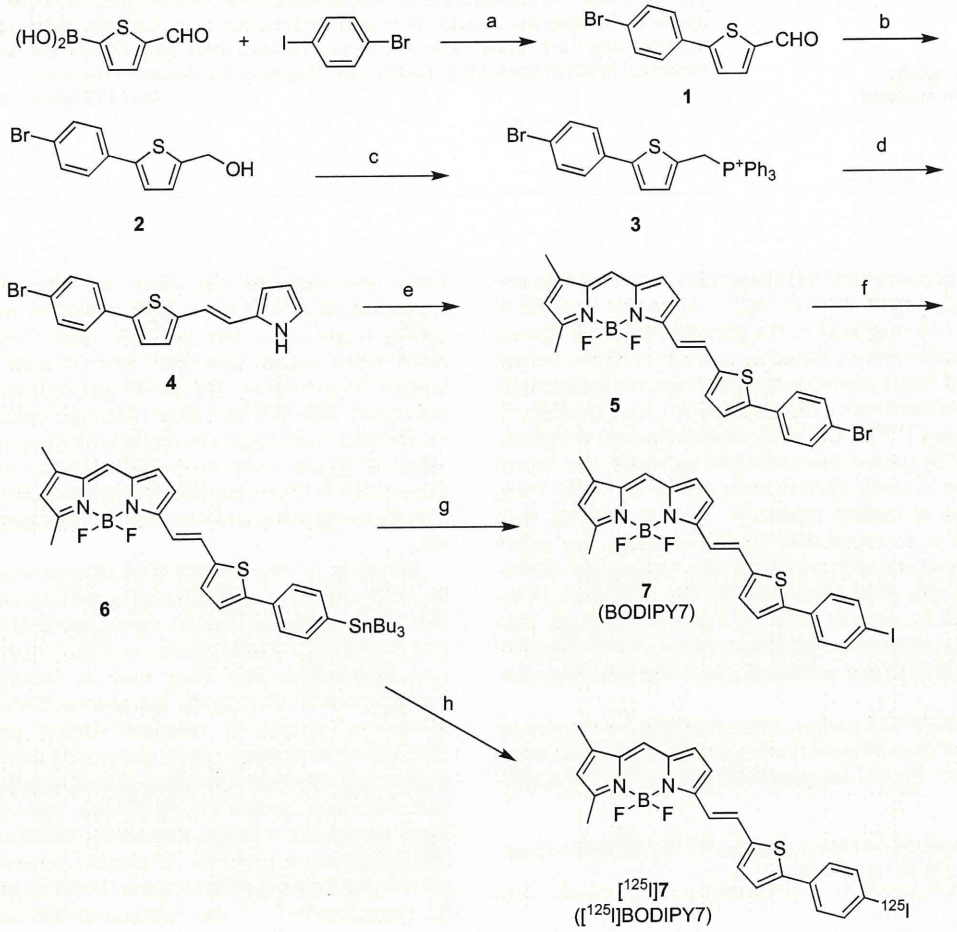

Scheme 1. Reagents: (a) dioxane, $(Ph_3P)_4Pd$, Na_2CO_3; (b) MeOH, $NaBH_4$; (c) $CHCl_3$, $Ph_3P{\cdot}HBr$; (d) MeOH, NaOMe, 2-formylpyrrole; (e) CH_2Cl_2, 3,5-dimethylpyrrole-2-carboxaldehyde, $POCl_3$, Et_3N, $EtOBF_3$; (f) dioxane, $(Bu_3Sn)_2$, $(Ph_3P)_4Pd$, Et_3N; (g) $CHCl_3$, I_2; (h) EtOH, HCl, H_2O_2, [^{125}I]NaI.

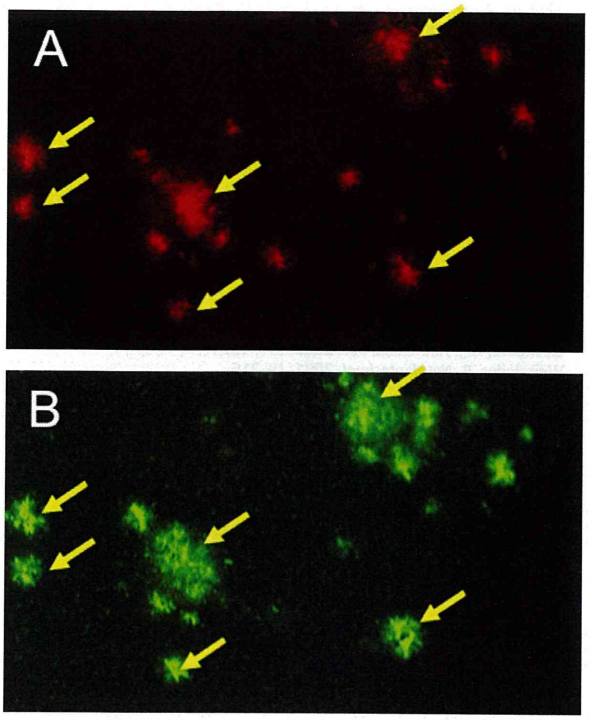

Figure 2. Neuropathological staining of BODIPY7 (A) in a 10-μm section from a Tg2576 mouse brain. Labeled plaques were confirmed by staining of the adjacent section with thioflavin S (B).

conformation, largely a neurotoxic form, of Aβ(1–42) soluble oligomers.[24] Although this Letter did not report the K_i value of the triazole-containing BODIPY, we consider BODIPY7 to potentially be suitable for monitoring conformational transitions of amyloid species in vitro. Also, these results support the validity of using BODIPY as a scaffold for probes to image Aβ plaques in vivo.

Next, the usefulness of BODIPY7 for neuropathological staining of Aβ plaques was investigated in an animal model of AD, the Tg2576 mouse, specifically engineered to overproduce Aβ plaques in the brain.[25] BODIPY7 clearly stained the plaques as reflected by its high affinity for Aβ aggregates in in vitro inhibition assays (Fig. 2A). The labeling pattern was consistent with that observed with thioflavin S (Fig. 2B). In contrast, wild-type mice displayed no remarkable accumulation of BODIPY7 in brain sections (data not shown). These results suggest that BODIPY7 can function as a probe for detecting Aβ plaques in the brain and deserves further investigation as a potential dual Aβ imaging probe.

Radioiodinated BODIPY7 was tested in normal mice to assess its ability to cross the blood–brain barrier (BBB) (Table 1). The uptake of [^{125}I]BODIPY7 in the brain was 0.4%ID/g at 2 min postinjection, and most radioactivity had been washed out from the brain by 30 min postinjection (0.14%ID/g). Biodistribution experiments also demonstrated high and persistent levels of radioactivity in the liver and spleen, and a decrease in uptake into the lung with time. Despite its suitable lipophilicity (log P = 2.2) and reasonable molecular size (mol wt 363),[10] the compound's uptake in the brain was relatively low, which may be explained by its rapid trapping in the liver. An initial brain uptake higher than 0.5%ID/organ at 2 min postinjection is preferred for Aβ imaging probes, and this initial uptake should remain at less than 30% at 30 min in normal mouse brain because of the absence of Aβ plaques. Although its initial uptakes fell short of these criteria, [^{125}I]BODIPY7 showed a rapid washout (30 min) with a value equal to 35% of the initial brain uptake. Despite good affinity for synthetic Aβ(1–42) aggregates

Table 1
Biodistribution of radioactivity after injection of [^{125}I]BODIPY7 in normal mice[a]

Tissue	Time after injection (min)			
	2	10	30	60
Blood	11.67 (1.70)	4.09 (0.25)	3.09 (0.17)	2.44 (1.25)
Liver	35.51 (3.62)	46.02 (1.80)	45.87 (2.60)	45.78 (3.58)
Kidney	5.39 (0.34)	4.79 (0.50)	4.46 (0.41)	4.43 (0.41)
Intestine	0.48 (0.07)	0.93 (0.16)	1.91 (0.17)	3.04 (0.18)
Spleen	16.12 (3.89)	26.90 (3.98)	28.21 (3.79)	21.52 (8.99)
Pancreas	1.19 (0.35)	0.74 (0.17)	0.72 (0.15)	0.92 (0.28)
Heart	5.59 (1.74)	2.95 (0.50)	2.31 (0.53)	2.30 (0.35)
Stomach[b]	1.40 (0.10)	4.73 (1.86)	4.79 (1.12)	5.50 (0.51)
Brain	0.40 (0.05)	0.19 (0.02)	0.14 (0.01)	0.14 (0.01)

[a] Expressed as% injection dose per gram. Each value represents the mean (SD) for 4–6 animals.
[b] Expressed as% injected dose per organ.

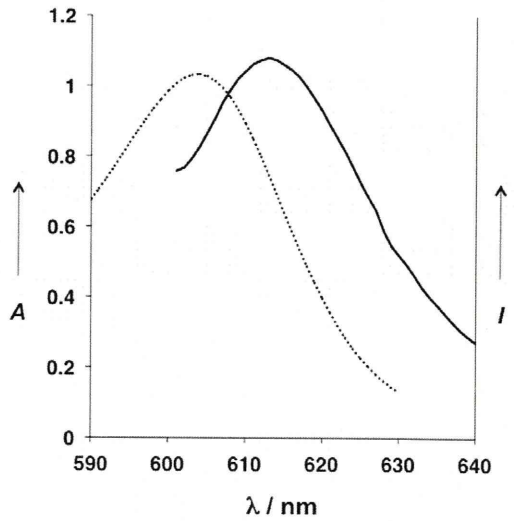

Figure 3. Absorption (dotted line) and emission (line) spectra of BODIPY7.

and the clear labeling of Aβ plaques in mouse brain sections, the radioiodinated BODIPY did not have characteristics for the imaging of Aβ plaques. Recently, it was reported that CRANAD-2 can penetrate the BBB and bind to Aβ plaques in the brain in vivo, though it possesses a difluoroboron core like BODIPY and a larger molecular weight than BODIPY7.[15] Therefore, additional structural changes may modify the properties of BODIPY derivatives to improve their suitability for imaging.

Although BODIPY7 had a high fluorescent quantum yield (φ = 0.36), it exhibited shorter wavelengths of absorption/emission at 606/613 nm than are appropriate for optical imaging in vivo (Fig. 3). Recent papers have reported the development of BODIPY derivatives with absorption/emission bands in the near-infrared region.[26] By introducing additional structural changes to extend the near-infrared wavelength simultaneously with modifications to improve penetration for the BBB, more useful SPECT/fluorescent probes may be developed in the future.

In conclusion, we designed and synthesized a radioiodinated BODIPY derivative as a dual SPECT/fluorescent probe for imaging Aβ plaques in the brain. In binding experiments in vitro, the BODIPY derivative showed high affinity for Aβ(1–42) aggregates. BODIPY7 clearly stained Aβ plaques in mouse brain, reflecting its affinity for Aβ aggregates in vitro. These findings suggest that additional structural changes to the BODIPY backbone may be applied to potential dual SPECT/fluorescent probes for the imaging of Aβ plaques.

Acknowledgments

This study was supported by the Program for Promotion of Fundamental Studies in Health Sciences of the National Institute of Biomedical Innovation (NIBIO), a Health Labour Sciences Research Grant, and a Grant-in-aid for Young Scientists (A) and Exploratory Research from the Ministry of Education, Culture, Sports, Science and Technology, Japan.

Supplementary data

Supplementary data (procedure for the preparation of new BODIPY derivatives, in vitro binding assay, in vitro fluorescent staining using Tg2576 mouse brain sections, and biodistribution studies) associated with this article can be found, in the online version, at doi:10.1016/j.bmcl.2010.05.027.

References and notes

1. Klunk, W. E. *Neurobiol. Aging* **1998**, *19*, 145.
2. Selkoe, D. J. *Physiol. Rev.* **2001**, *81*, 741.
3. Mathis, C. A.; Wang, Y.; Holt, D. P.; Huang, G. F.; Debnath, M. L.; Klunk, W. E. *J. Med. Chem.* **2003**, *46*, 2740.
4. O'Keefe, G. J.; Saunder, T. H.; Ng, S.; Ackerman, U.; Tochon-Danguy, H. J.; Chan, J. G.; Gong, S.; Dyrks, T.; Lindemann, S.; Holl, G.; Dinkelborg, L.; Villemagne, V.; Rowe, C. C. *J. Nucl. Med.* **2009**, *50*, 309.
5. Johnson, A. E.; Jeppsson, F.; Sandell, J.; Wensbo, D.; Neelissen, J. A.; Jureus, A.; Strom, P.; Norman, H.; Farde, L.; Svensson, S. P. *J. Neurochem.* **2009**, *108*, 1177.
6. Choi, S. R.; Golding, G.; Zhuang, Z.; Zhang, W.; Lim, N.; Hefti, F.; Benedum, T. E.; Kilbourn, M. R.; Skovronsky, D.; Kung, H. F. *J. Nucl. Med.* **2009**, *50*, 1887.
7. Newberg, A. B.; Wintering, N. A.; Clark, C. M.; Plossl, K.; Skovronsky, D.; Seibyl, J. P.; Kung, M. P.; Kung, H. F. *J. Nucl. Med.* **2006**, *47*, 78P.
8. Kung, M. P.; Hou, C.; Zhuang, Z. P.; Zhang, B.; Skovronsky, D.; Trojanowski, J. Q.; Lee, V. M.; Kung, H. F. *Brain Res.* **2002**, *956*, 202.
9. Scheinin, N. M.; Aalto, S.; Koikkalainen, J.; Lotjonen, J.; Karrasch, M.; Kemppainen, N.; Viitanen, M.; Nagren, K.; Helin, S.; Scheinin, M.; Rinne, J. O. *Neurology* **2009**, *73*, 1186.
10. Mathis, C. A.; Wang, Y.; Klunk, W. E. *Curr. Pharm. Des.* **2004**, *10*, 1469.
11. Weissleder, R.; Mahmood, U. *Radiology* **2001**, *219*, 316.
12. Hintersteiner, M.; Enz, A.; Frey, P.; Jaton, A. L.; Kinzy, W.; Kneuer, R.; Neumann, U.; Rudin, M.; Staufenbiel, M.; Stoeckli, M.; Wiederhold, K. H.; Gremlich, H. U. *Nat. Biotechnol.* **2005**, *23*, 577.
13. Nesterov, E. E.; Skoch, J.; Hyman, B. T.; Klunk, W. E.; Bacskai, B. J.; Swager, T. M. *Angew. Chem. Int., Ed. Engl.* **2005**, *44*, 5452.
14. Raymond, S. B.; Skoch, J.; Hills, I. D.; Nesterov, E. E.; Swager, T. M.; Bacskai, B. J. *Eur. J. Nucl. Med. Mol. Imaging* **2008**, *35*, S93.
15. Ran, C.; Xu, X.; Raymond, S. B.; Ferrara, B. J.; Neal, K.; Bacskai, B. J.; Medarova, Z.; Moore, A. *J. Am. Chem. Soc.* **2009**, *131*, 15257.
16. Weissleder, R. *Nat. Biotechnol.* **2001**, *19*, 316.
17. Li, C.; Wang, W.; Wu, Q.; Ke, S.; Houston, J.; Sevick-Muraca, E.; Dong, L.; Chow, D.; Charnsangavej, C.; Gelovani, J. G. *Nucl. Med. Biol.* **2006**, *33*, 349.
18. Bhushan, K. R.; Misra, P.; Liu, F.; Mathur, S.; Lenkinski, R. E.; Frangioni, J. V. *J. Am. Chem. Soc.* **2008**, *130*, 17648.
19. Loudet, A.; Burgess, K. *Chem. Rev.* **2007**, *107*, 4891.
20. Nagai, A.; Miyake, J.; Kokado, K.; Nagata, Y.; Chujo, Y. J. *J. Am. Chem. Soc.* **2008**, *130*, 15276.
21. Sun, Z. N.; Liu, F. Q.; Chen, Y.; Tam, P. K.; Yang, D. *Org. Lett.* **2008**, *10*, 2171.
22. Lee, J. S.; Kang, N. Y.; Kim, Y. K.; Samanta, A.; Feng, S.; Kim, H. K.; Vendrell, M.; Park, J. H.; Chang, Y. T. *J. Am. Chem. Soc.* **2009**, *131*, 10077.
23. Ojida, A.; Sakamoto, T.; Inoue, M. A.; Fujishima, S. H.; Lippens, G.; Hamachi, I. *J. Am. Chem. Soc.* **2009**, *131*, 6543.
24. Smith, N. W.; Alonso, A.; Brown, C. M.; Dzyuba, S. V. *Biochem. Biophys. Res. Commun.* **2009**, *391*, 1455.
25. Hsiao, K.; Chapman, P.; Nilsen, S.; Eckman, C.; Harigaya, Y.; Younkin, S.; Yang, F.; Cole, G. *Science* **1996**, *274*, 99.
26. Umezawa, K.; Matsui, A.; Nakamura, Y.; Citterio, D.; Suzuki, K. *Chemistry* **2009**, *15*, 1096.

Bioorganic & Medicinal Chemistry 18 (2010) 4740–4746

Contents lists available at ScienceDirect

Bioorganic & Medicinal Chemistry

journal homepage: www.elsevier.com/locate/bmc

Synthesis and characterization of novel phenylindoles as potential probes for imaging of β-amyloid plaques in the brain

Hiroyuki Watanabe [a], Masahiro Ono [a,b,*], Mamoru Haratake [a], Nobuya Kobashi [a], Hideo Saji [b], Morio Nakayama [a,*]

[a] Department of Hygienic Chemistry, Graduate School of Biomedical Sciences, Nagasaki University, 1-14 Bunkyo-machi, Nagasaki 852-8521, Japan
[b] Department of Patho-Functional Bioanalysis, Graduate School of Pharmaceutical Sciences, Kyoto University, Yoshida Shimoadachi-cho, Sakyo-ku, Kyoto 606-8501, Japan

ARTICLE INFO

Article history:
Received 6 April 2010
Revised 1 May 2010
Accepted 4 May 2010
Available online 13 May 2010

Keywords:
Alzheimer's disease
β-amyloid
Imaging
Phenylindole

ABSTRACT

We synthesized a novel series of phenylindole (PI) derivatives and evaluated their biological activities as probes for imaging Aβ plaques in vivo. The affinity for Aβ plaques was assessed by an in vitro-binding assay using pre-formed synthetic Aβ aggregates. 2-Phenyl-1*H*-indole (2-PI) derivatives showed high affinity for Aβ42 aggregates with K_i values ranging from 4 to 32 nM. 2-PI derivatives clearly stained Aβ plaques in an animal model of AD. In biodistribution experiments using normal mice, 2-PI derivatives displayed sufficient uptake for imaging, ranging from 1.1% to 2.6% ID/g. Although additional modifications are necessary to improve uptake by and clearance from the brain, 2-PI derivatives may be useful as a backbone structure to develop novel Aβ imaging agents.

1. Introduction

Alzheimer's disease (AD) is the most common neurodegenerative disorder of the elderly and is characterized clinically by dementia, cognitive impairment, and memory loss. Postmortem brains of AD patients reveal neuropathological features: the presence of senile plaques and neurofibrillary tangles, which contain β-amyloid (Aβ) peptides and highly phosphorylated tau proteins.[1,2] The formation and deposition of Aβ plaques is considered one of the most significant factors in AD. Currently, the only definitive diagnosis of AD is by pathological examination of postmortem staining of affected brain tissue. Therefore, non-invasive techniques such as positron emission tomography (PET) and single photon emission computed tomography (SPECT) are useful for the diagnosis of AD and new anti-amyloid therapies.[3–5]

Many radiolabeled probes based on the core structure of Congo Red (CR) and thioflavin T (ThT) have been developed as imaging agents for Aβ plaques. Although CR has large molecular size, some truncated CR type molecules such as stilbene and styrylpyridine derivatives have been reported.[6–8] Because ThT has a lower molecular weight than CR, implying greater blood–brain penetration and easier organic synthesis, a number of groups have worked to develop probes for PET/SPECT derived from ThT including [^{11}C]PIB,[9,10] [^{11}C]AZD2184,[11,12] TZDM,[13] IBOX,[14] [^{123}I]IMPY,[15,16] phenylbenzofuran derivatives,[17,18] phenylbenzothiophene derivatives,[19] imidazopyridine derivatives,[20,21] and imidazopyridazine derivatives[22] (Fig. 1). Clinical trials in AD patients have been conducted with [^{11}C]PIB and [^{11}C]AZD2184, and indicated the PET-based imaging of Aβ plaques in the living human brain to be useful for the diagnosis of AD. Radioiodinated probes for SPECT such as TZDM, IBOX, and phenylbenzofuran derivatives have shown high affinity for Aβ aggregates in vitro and high initial uptake, but a slow washout from the brain.[13,14,17] Since the slow washout leads to a low signal/noise ratio in the imaging of Aβ plaques in vivo, a molecular design that facilitates the clearance of the radiolabeled probes from normal areas of the brain is needed. Several reports have shown the lipophilicity of probes to play an important role in uptake by and clearance from brain tissue.[9,23] As this may partly explain the slow washout from the brain, we planned to select a ThT-derived scaffold with less lipophilicity. In the search for such a scaffold, we focused on phenylindole, never before applied to the development of Aβ imaging probes, and calculated its log *D* value to be 3.97, lower than that of phenylbenzofuran (4.34) or phenylbenzothiophene (4.94) (calculated with the Sparc On-Line Calculator).

In the present study, we synthesized a novel series of 2-phenyl-1*H*-indole (2-PI) and 1-phenyl-1*H*-indole (1-PI) derivatives and evaluated their potential as probes for imaging Aβ in vivo. This is the first time that PI derivatives have been used for SPECT to detect Aβ plaques.

* Corresponding authors. Tel.: +81 75 753 4608; fax: +81 75 753 4568 (M.O.); tel./fax: +81 95 819 2441 (M.N.).
E-mail addresses: ono@pharm.kyoto-u.ac.jp (M. Ono), morio@nagasaki-u.ac.jp (M. Nakayama).

0968-0896/$ - see front matter © 2010 Elsevier Ltd. All rights reserved.
doi:10.1016/j.bmc.2010.05.013

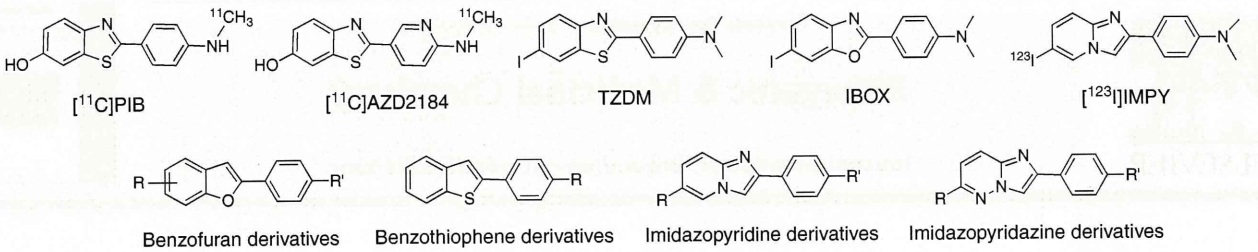

Figure 1. Chemical structure of thioflavin T analogs.

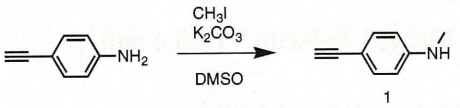

Scheme 1.

2. Results and discussion

The synthesis of 2-PI derivatives is outlined in Schemes 1–4. We used a one-pot method producing 2-PI.[24] Compounds **3**, **6**, and **12** were prepared from **2** and terminal alkynes (**1**, 4-ethynyl-*N*,*N*-dimethylaniline and *p*-ethynylanisole) using a palladium catalyst in the presence of tetrabutylammonium fluoride (TBAF) (27.2–49.5% yields). Trimethyltin derivatives (**4**, **7**, and **13**) were prepared from the corresponding bromo compounds (**3**, **6**, and **12**) using a bromo-to-trimethyltin exchange reaction catalyzed by Pd(0). Trimethyltin derivatives (**4** and **13**) were readily reacted with iodine in ethyl acetate at room temperature to give the iodo derivatives, **5** and **14**. The tributyltin derivative **9** was prepared from the corresponding bromo compound by protecting the *tert*-butoxycarbonyl (Boc) group. Compound **9** was readily reacted with iodine in ethyl acetate at room temperature to give the iodo derivative **10** and deprotected by TFA. Compounds **12** and **14** were converted to **17** and **15** by demethylation with BBr_3 in CH_2Cl_2 (13.0% and 19.5% yields), respectively. Direct alkylation of **17** and **15** with ethylene chlorohydrin and potassium carbonate in DMF resulted in **18** and **16**, respectively. The synthesis of 1-PI derivatives is outlined in Scheme 5. Compound **20** was prepared by the copper-mediated coupling of a substituted indole with 4-(dimethylamino)phenylboronic acid in a yield of 44.2%.[25] The tributyltin derivative **21** was readily reacted with iodine in ethyl acetate at room temperature to give the iodo derivative **22**. The trimethyltin derivatives were

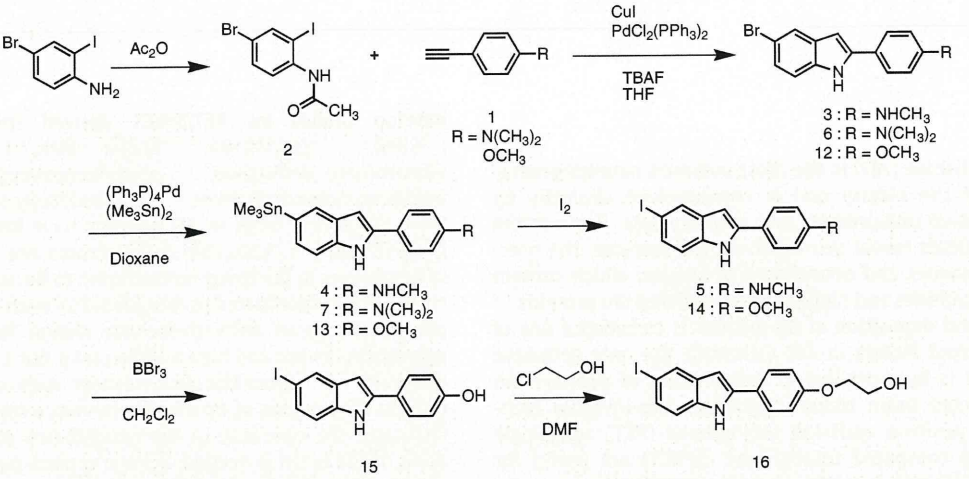

Scheme 2.

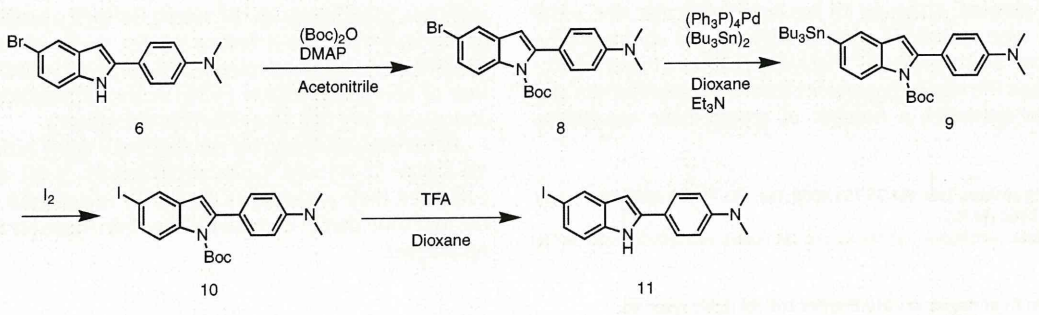

Scheme 3.

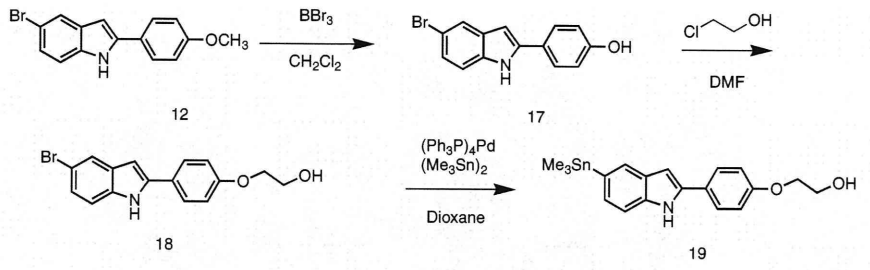

Scheme 4.

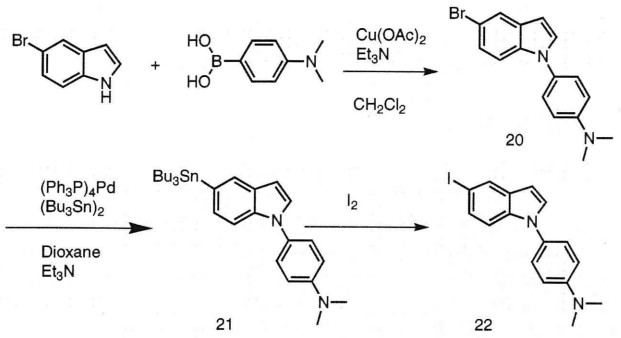

Scheme 5.

used as the starting materials for radioiodination in the preparation of [^{125}I]**5**, [^{125}I]**11**, [^{125}I]**14**, and [^{125}I]**16**. Novel radioiodinated 2-PI derivatives were obtained by iododestannylation reactions using NCS as an oxidant (Scheme 6). It was anticipated that not adding a carrier would result in a final product bearing a theoretical specific activity similar to that of ^{125}I (2200 Ci/mmol). The radiochemical identity of the radioiodinated ligands was verified by co-injection with non-radioiodinated compounds from HPLC profiles. The HPLC retention times are shown in Supplementary data. [^{125}I]**5**, [^{125}I]**11**, [^{125}I]**14**, and [^{125}I]**16** were each obtained in a radiochemical yield of 14–56% with a radiochemical purity of >95% after purification by HPLC.

The affinity of PI derivatives (**5**, **11**, **14**, **15**, **16**, and **22**) was evaluated based on inhibition of the binding of [^{125}I]IMPY to Aβ42 aggregates. The 2-PI derivatives (**5**, **11**, **14**, **15**, and **16**) showed inhibitory activity toward Aβ aggregates, while the 1-PI derivative **22** did not (Table 1 and Fig. 2). The K_i values of **5**, **11**, **14**, **15**, and **16** were 27, 4, 20, 33, and 26 nM, respectively, suggesting high affinity for Aβ(1–42) aggregates and considerable tolerance of structural modifications. They also suggested that the position of the substituted phenyl group in the PI molecule plays an important role in the affinity for Aβ aggregates.

To confirm the affinity of the 2-PI derivatives for Aβ plaques in the brain, fluorescent staining of sections of brain tissue from an animal model of AD was carried out with **11** (Fig. 3). Many specks of fluorescence were observed in brain sections of *Tg2576*

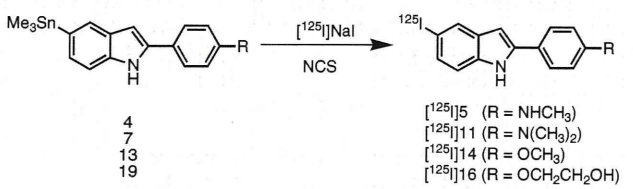

Scheme 6.

Table 1
Inhibition constants (K_i) for binding of PI derivatives determined using [^{125}I]IMPY as the ligand in Aβ(1–42) aggregates

Compound	K_i (nM)[a]
5	27.0 ± 0.18
11	4.24 ± 0.71
14	20.2 ± 5.15
15	32.9 ± 2.93
16	25.9 ± 5.13
22	>10,000

[a] Values are means ± standard error of the mean for 3–6 independent experiments.

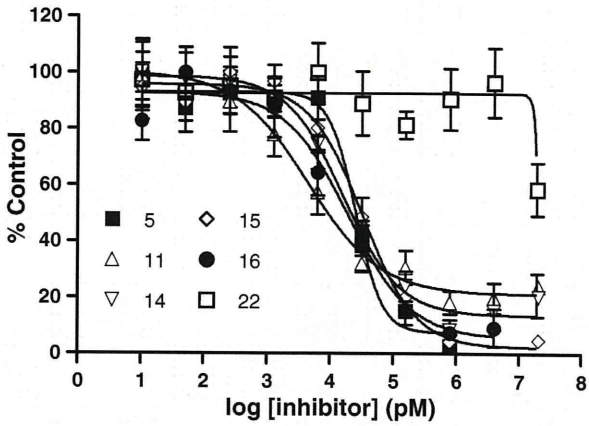

Figure 2. Curves of [^{125}I]IMPY against 2-PI (**5**, **11**, **14**, **15**, and **16**) and 1-PI (**22**).

transgenic mice (female, 28 months old) (Fig. 3A), while none were observed in wild-type mice (female, 22 months old) (Fig. 3B). The pattern of labeling was consistent with that observed with thioflavin S (Fig. 3C). Compound **11** should therefore show specific binding to Aβ plaques in the mouse brain. Compound **14** also clearly stained Aβ plaques in the *Tg2576* mouse brain (data not shown). A slight difference in K_i of **11** and **14** did not significantly affect the staining in mouse brain sections.

To evaluate the uptake into the brain of the PI derivatives, biodistribution experiments were performed in normal mice with four radioiodinated PI derivatives; [^{125}I]**5**, [^{125}I]**11**, [^{125}I]**14**, and [^{125}I]**16** (Table 2). Radioactivity penetrated the blood–brain barrier with the rate of uptake ranging from 1.2% to 2.6% ID/g brain at 2–10 min postinjection. But the washout of these probes from the brain in normal mice appears to be relatively slow. The uptake of [^{125}I]**11** was higher in the stomach than in any other organ, possibly due to deiodination. The brain uptake and clearance is similar to that of radioiodinated ThT analogs such as TZDM and IBOX.[13,14] More recently, we have developed ^{11}C-labeled phenylbenzofuran derivative, which are less lipophilic by replacing the iodine with a

Figure 3. Neuropathological staining of **11** in 10-μm AD model mouse sections (A) and wild-type mouse sections (B). Labeled plaques were confirmed by staining of the adjacent sections with thioflavin S (C).

Table 2
Biodistribution of radioactivity after injection of [^{125}I]2-PI derivatives in normal mice[a]

Tissue	Time after injection (min)			
	2	10	30	60
*[^{125}I]**5***				
Blood	3.77 (1.25)	1.71 (0.15)	1.36 (0.15)	0.80 (0.13)
Liver	22.85 (9.60)	26.83 (1.28)	23.07 (2.33)	15.89 (6.13)
Kidney	5.53 (1.77)	4.31 (0.44)	3.84 (0.67)	2.61 (0.86)
Intestine	0.97 (0.33)	3.57 (0.34)	8.54 (1.80)	9.48 (1.88)
Spleen	7.83 (2.24)	19.67 (8.82)	10.34 (1.26)	5.89 (3.27)
Pancreas	2.31 (0.70)	2.87 (0.33)	2.12 (0.32)	1.27 (0.23)
Heart	5.68 (1.27)	3.59 (0.29)	2.96 (0.42)	1.88 (0.57)
Stomach[b]	0.52 (0.03)	1.34 (0.53)	2.55 (2.12)	1.68 (0.53)
Brain	1.10 (0.27)	1.68 (0.13)	1.42 (0.03)	0.83 (0.17)
*[^{125}I]**11***				
Blood	6.18 (0.65)	4.53 (0.37)	3.68 (0.41)	3.29 (1.00)
Liver	10.20 (1.92)	5.14 (1.01)	3.55 (0.62)	3.24 (0.76)
Kidney	9.49 (1.61)	4.46 (0.71)	4.58 (1.24)	4.71 (2.44)
Intestine	1.80 (0.24)	3.09 (0.40)	4.52 (0.58)	6.08 (1.58)
Spleen	4.13 (0.64)	3.28 (0.57)	2.60 (0.41)	2.24 (0.64)
Pancreas	5.21 (2.50)	4.13 (0.67)	3.10 (0.41)	2.30 (0.54)
Heart	8.08 (1.59)	4.82 (0.67)	1.87 (0.21)	1.84 (0.76)
Stomach[b]	4.03 (0.65)	10.65 (2.18)	17.77 (2.04)	16.26 (3.52)
Brain	1.19 (0.34)	1.19 (0.30)	0.96 (0.17)	0.71 (0.19)
*[^{125}I]**14***				
Blood	3.59 (1.41)	1.97 (0.54)	1.38 (0.25)	0.74 (0.37)
Liver	17.81 (5.73)	13.96 (4.21)	10.38 (2.64)	8.22 (1.87)
Kidney	8.76 (2.19)	4.96 (1.44)	2.89 (0.44)	2.05 (0.54)
Intestine	1.90 (0.66)	6.85 (1.86)	12.32 (3.65)	20.35 (5.86)
Spleen	4.22 (0.78)	3.43 (1.15)	2.96 (0.41)	2.02 (0.92)
Pancreas	4.54 (0.44)	3.94 (1.46)	1.95 (0.33)	1.29 (0.37)
Heart	7.72 (1.94)	2.97 (1.26)	1.47 (0.20)	1.06 (0.42)
Stomach[b]	0.72 (0.39)	1.38 (1.42)	2.67 (3.24)	3.06 (1.28)
Brain	2.11 (0.69)	2.07 (0.71)	1.36 (0.37)	1.16 (0.32)
*[^{125}I]**16***				
Blood	4.07 (0.30)	1.60 (0.30)	1.26 (0.26)	0.80 (0.20)
Liver	17.69 (2.64)	16.77 (2.20)	13.42 (1.70)	8.17 (1.28)
Kidney	11.93 (1.83)	9.35 (0.46)	6.77 (0.83)	2.76 (0.45)
Intestine	1.97 (0.22)	5.76 (0.66)	11.32 (1.65)	18.98 (3.21)
Spleen	7.56 (1.24)	7.09 (1.60)	4.75 (0.82)	2.39 (0.52)
Pancreas	5.55 (1.00)	5.59 (0.56)	3.57 (0.40)	2.22 (0.29)
Heart	12.91 (2.16)	5.84 (0.36)	2.97 (0.62)	1.36 (0.17)
Stomach[b]	0.97 (0.31)	1.97 (1.05)	2.11 (0.26)	1.62 (0.44)
Brain	2.13 (0.54)	2.62 (0.21)	1.93 (0.18)	1.82 (0.35)

[a] Expressed as % injected dose per gram. Each value represents the mean (SD) for 3–5 animals.
[b] Expressed as % injected dose per organ.

hydroxy group.[18] [^{11}C]Phenylbenzofuran, which has less lipophilicity than [^{125}I]phenylbenzofuran, showed a higher and faster peak of brain uptake and faster washout in normal mice. The improved properties of [^{11}C]phenylbenzofuran derivatives could make them a better candidate for the imaging of Aβ plaques. Similar to [^{125}I]phenylbenzofuran, the 2-PI derivatives had unfavorable in vivo pharmacokinetics in normal mice, despite their good affinity for Aβ aggregates. Additional structural changes, that is, reducing the lipophilicity by introducing a hydrophilic group, are necessary to improve the properties of 2-PI derivatives.

3. Conclusion

We developed PI derivatives as novel SPECT ligands for imaging Aβ plaques in the AD brain. 2-PI derivatives (**5**, **11**, **14**, **15**, and **16**) displayed excellent affinity for Aβ in binding experiments in vitro. They clearly stained Aβ plaques in *Tg2576* mouse brain, reflecting their affinity for Aβ aggregates in vitro. The degree to which the 2-PI derivatives penetrated the brain was very encouraging. However, non-specific binding in vivo reflected by a slow washout from the normal mouse brain may make them unsuitable for the imaging of Aβ plaques. In in vivo biodistribution results in normal mice indicate that there is a critical need to fine-tune the kinetics of brain uptake and washout. Additional changes to 2-PI may lead to useful probes for detecting Aβ plaques in the AD brain.

4. Experimental

4.1. General

All reagents were commercial products and used without further purification unless otherwise indicated. ^{1}H NMR spectra were obtained on a Varian Gemini 300 spectrometer with TMS as an internal standard. Coupling constants are reported in hertz. Multiplicity was defined by s (singlet), d (doublet), t (triplet), and m (multiplet). Mass spectra were obtained on a JEOL IMS-DX.

4.1.1. 4-Ethynyl-*N*-methylbenzenamine (1)

To a solution of 4-ethynylaniline (819 mg, 7 mmol) in DMSO were added methyl iodide (1.3 mL, 21 mmol) and anhydrous K_2CO_3 (4.8 g, 35 mmol). The reaction mixture was stirred at room temperature for 3 h. After it was poured into water, the mixture was extracted with ethyl acetate. The organic layers were dried over Na_2SO_4. The solvent was removed and the residue was purified by silica gel chromatography (hexane/ethyl acetate = 2:1) to give 313 mg of **1** (34.1%). ^{1}H NMR (300 MHz, $CDCl_3$) δ 2.49 (s, 1H), 2.83 (s, 3H), (s, 1H), 6.50 (d, J = 8.7 Hz, 2H), 7.32 (d, J = 8.7 Hz, 2H).

4.1.2. *N*-(4-Bromo-2-iodophenyl)acetamide (2)

A mixture of 4-bromo-2-iodoaniline (586 mg, 2 mmol) and acetic anhydride (0.19 mL, 2 mmol) in toluene (5 mL) was stirred at room temperature for 3.5 h. The solid that formed was filtered and washed with hexane to give 464 mg of **2** (69.4%). ^{1}H NMR (300 MHz, $CDCl_3$) δ 2.24 (s, 3H), 7.39 (s, 1H), 7.46 (dd, J = 2.4, 2.1 Hz, 1H), 7.90 (d, J = 2.1 Hz, 1H), 8.13 (d, J = 8.7 Hz, 1H).

4.1.3. 4-(5-Bromo-1*H*-indol-2-yl)-*N*-methylbenzenamine (3)

A mixture of **1** (313 mg, 2.4 mmol), **2** (396 mg, 1.2 mmol), $PdCl_2(PPh_3)$ (60 mg, 0.06 mmol), CuI (50 mg, 0.22 mmol), THF

(5 mL), and TBAF (1 M solution in THF, 5 mL) was stirred under reflux for 5 h. After removal of the THF, the residue was diluted with water and extracted with ethyl acetate, and the organic phase was dried over Na_2SO_4. The solvent was removed and the residue was purified by silica gel chromatography (hexane/ethyl acetate = 2:1) to give 179 mg of **3** (49.5%). ^{1}H NMR (300 MHz, $CDCl_3$) δ 2.90 (s, 3H), 6.57 (d, J = 2.4 Hz, 1H), 6.67 (d, J = 8.7 Hz, 2H), 7.21 (s, 2H), 7.49 (d, J = 8.7 Hz, 2H), 7.69 (s, 1H) 8.25 (s, 1H).

4.1.4. *N*-Methyl-4-(5-(trimethylstannyl)-1*H*-indol-2-yl) benzenamine (4)

A mixture of **3** (179 mg, 0.59 mmol), $Pd(PPh_3)_4$ (88 mg, 0.077 mmol) and $(Me_3Sn)_2$ (198 mg, 0.6 mmol) in 1,4-dioxane (5 mL) was stirred under reflux for 3.5 h. The solvent was removed and the residue was purified by silica gel chromatography (hexane/ethyl acetate = 3:1) to give 6 mg of **4** (2.1%). ^{1}H NMR (300 MHz, $CDCl_3$) δ 0.30 (s, 9H), 2.88 (s, 3H), 3.84 (s, 1H), 6.62 (s, 1H), 6.67 (d, J = 8.7 Hz, 2H), 7.22 (d, J = 9.0 Hz, 1H), 7.37 (d, J = 7.8 Hz, 1H), 7.50 (d, J = 9.0 Hz, 2H), 7.70 (s, 1H), 8.18 (s, 1H).

4.1.5. 4-(5-Iodo-1*H*-indol-2-yl)-*N*-methylbenzenamine (5)

To a solution of **4** (9 mg, 0.019 mmol) in ethyl acetate (1 mL) was added a solution of iodine in ethyl acetate (1 mL, 0.25 M) at room temperature. The mixture was stirred for 15 s, and $NaHSO_3$ solution (1 mL) was added. The organic phase was separated and dried over Na_2SO_4. The solvent was removed and the residue was purified by silica gel chromatography (hexane/ethyl acetate = 3:1) to give 5 mg of **5** (77.4%). ^{1}H NMR (300 MHz, $CDCl_3$) δ 2.89 (s, 3H), 6.56 (s, 1H), 6.67 (d, J = 8.7 Hz, 2H), 7.13 (d, J = 8.1 Hz, 1H), 7.37 (dd, J = 1.8, 1.8 Hz, 1H), 7.48 (d, J = 9.0 Hz, 1H) 7.90 (s, 1H), 8.23 (s, 1H). HRMS m/z $C_{15}H_{13}N_2I$ found 348.0109/calcd 348.0123 (M^+).

4.1.6. 4-(5-Bromo-1*H*-indol-2-yl)-*N*,*N*-dimethylbenzenamine (6)

The same reaction as described above to prepare **3** was used, and 25 mg of **6** was obtained in a 27.2% yield from **2** (99 mg, 0.3 mmol) and 4-ethynyl-*N*,*N*-dimethylaniline (65 mg, 0.45 mmol). ^{1}H NMR (300 MHz, $CDCl_3$) δ 3.02 (s, 6H), 6.59 (d, J = 1.8 Hz, 1H), 6.78 (d, J = 9.0 Hz, 2H), 7.21–7.22 (m, 2H), 7.53 (d, J = 9.0 Hz, 2H), 7.68 (s, 1H) 8.27 (s, 1H).

4.1.7. *N*,*N*-Dimethyl-4-(5-(trimethylstannyl)-1*H*-indol-2-yl) benzenamine (7)

The same reaction as described above to prepare **4** was used, and 2 mg of **7** was obtained in a 7.1% yield from **6** (22 mg, 0.07 mmol). ^{1}H NMR (300 MHz, $CDCl_3$) δ 0.31 (s, 9H), 3.01 (s, 6H), 6.64 (s, 1H), 6.79 (d, J = 9.3 Hz, 2H), 7.23 (d, J = 6.9 Hz, 1H), 7.38 (d, J = 8.1 Hz, 1H), 7.55 (d, J = 9.0 Hz, 2H), 7.71 (s, 1H), 8.21 (s, 1H).

4.1.8. *tert*-Butyl 5-bromo-2-(4-(dimethylamino)phenyl)-1*H*-indole-1-carboxylate (8)

$(Boc)_2O$ (159 mg, 0.73 mmol) was added to a solution of **7** (41 mg, 0.13 mmol) and 4-(*N*,*N*-dimethylamino)pyridine (DMAP) (4.8 mg, 0.004 mmol) in acetonitrile. The reaction mixture was stirred at room temperature for 3 h. After it was poured into water, the mixture was extracted with ethyl acetate. The organic layers were dried over Na_2SO_4. The solvent was removed and the residue was purified by silica gel chromatography (hexane/ethyl acetate = 4:1) to give 54 mg of **8** (100%). ^{1}H NMR (300 MHz, $CDCl_3$) δ 1.38 (s, 9H), 3.00 (s, 6H), 6.41 (s, 1H), 6.75 (d, J = 8.4 Hz, 2H), 7.29 (s, 2H), 7.36 (d, J = 9.0 Hz, 1H), 7.63 (s, 1H) 8.02 (d, J = 8.7 Hz, 1H).

4.1.9. *tert*-Butyl 5-(tributylstannyl)-2-(4-(dimethylamino) phenyl)-1*H*-indole-1-carboxylate (9)

A mixture of **8** (54 mg, 0.13 mmol), $(Bu_3Sn)_2$ (0.3 mL) and $(Ph_3P)_4Pd$ (16 mg, 0.01 mmol) in a mixed solvent (6 mL, 1:1 = 1,4-dioxane/Et_3N) was stirred under reflux for 11 h. The solvent was removed, and the residue was purified by silica gel chromatography (hexane/ethyl acetate = 9:1) to give 20 mg of **9** (12.4%). ^{1}H NMR (300 MHz, $CDCl_3$) δ 0.84–1.61 (m, 36H), 2.99 (s, 6H), 6.46 (s, 1H), 6.75 (d, J = 8.7 Hz, 2H), 7.29 (d, J = 8.4 Hz, 2H), 7.35 (d, J = 8.1 Hz, 1H), 7.61 (s, 1H), 8.11 (d, J = 7.5 Hz, 1H).

4.1.10. *tert*-Butyl 2-(4-(dimethylamino)phenyl)-5-iodo-1*H*-indole-1-carboxylate (10)

The same reaction as described above to prepare **5** was used, and 10 mg of **10** was obtained in a 67.6% yield from **9** (20 mg, 0.03 mmol). ^{1}H NMR (300 MHz, $CDCl_3$) δ 1.37 (s, 9H), 3.00 (s, 3H), 6.39 (s, 1H), 6.74 (d, J = 8.7 Hz, 2H), 7.29 (s, 2H), 7.53 (dd, J = 1.8, 1.8 Hz, 1H) 7.84 (d, J = 2.1 Hz, 1H), 7.91 (d, J = 9.0 Hz, 1H).

4.1.11. 4-(5-Iodo-1*H*-indol-2-yl)-*N*,*N*-dimethylbenzenamine (11)

To a solution of **10** (71 mg, 0.15 mmol) in CH_2Cl_2 (2 mL) was added TFA (300 μL) at room temperature. After the mixture was stirred for 3 h, the solvent was removed. The residue was purified by preparative TLC (hexane/ethyl acetate = 3:1) to give 13 mg of **11** (27.0%). ^{1}H NMR (300 MHz, $CDCl_3$) δ 3.02 (s, 6H), 6.57 (s, 1H), 6.79 (d, J = 8.7 Hz, 2H), 7.14 (d, J = 8.7 Hz, 1H), 7.36 (dd, J = 1.5, 1.5 Hz, 1H), 7.53 (d, J = 9.0 Hz, 1H), 7.89 (s, 1H), 8.28 (s, 1H). HRMS m/z $C_{16}H_{15}N_2I$ found 362.0278/calcd 362.0280 (M^+).

4.1.12. 5-Bromo-2-(4-methoxyphenyl)-1*H*-indole (12)

The same reaction as described above to prepare **3** was used, and 54 mg of **12** was obtained in a 30.7% yield from **2** (198 mg, 0.6 mmol) and *p*-ethynylanisole (116 μL, 0.9 mmol). ^{1}H NMR (300 MHz, $CDCl_3$) δ 3.87 (s, 3H), 6.50 (s, 1H), 6.99 (d, J = 8.7 Hz, 2H), 7.25 (s, 2H), 7.59 (d, J = 8.7 Hz, 2H), 7.12 (s, 1H), 8.30 (s, 1H).

4.1.13. 2-(4-Methoxyphenyl)-5-(trimethylstannyl)-1*H*-indole (13)

The same reaction as described above to prepare **4** was used, and 15 mg of **13** was obtained in a 23.9% yield from **12** (49 mg, 0.16 mmol). ^{1}H NMR (300 MHz, $CDCl_3$) δ 0.30 (s, 9H), 3.86 (s, 3H), 6.68 (s, 1H), 6.98 (d, J = 9.0 Hz, 2H), 7.26 (d, J = 7.2 Hz, 1H), 7.39 (d, J = 7.8 Hz, 1H), 7.59 (d, J = 9.0 Hz, 2H), 7.73 (s, 1H), 8.22 (s, 1H).

4.1.14. 5-Iodo-2-(4-methoxyphenyl)-1*H*-indole (14)

The same reaction as described above to prepare **5** was used, and 9 mg of **14** was obtained in a 66.3% yield from **13** (15 mg, 0.039 mmol). ^{1}H NMR (300 MHz, $CDCl_3$) δ 3.86 (s, 3H), 6.63 (s, 1H), 6.99 (d, J = 9.0 Hz, 2H), 7.16 (d, J = 8.4 Hz, 1H), 7.41 (dd, J = 1.8, 1.5 Hz, 1H), 7.58 (d, J = 8.7 Hz, 2H), 7.93 (s, 1H), 8.29 (s, 1H). HRMS m/z $C_{15}H_{12}NOI$ found 348.9962/calcd 348.9964 (M^+).

4.1.15. 4-(5-Iodo-1*H*-indol-2-yl)phenol (15)

BBr_3 (0.7 mL, 1 M solution in CH_2Cl_2) was added to a solution of **14** (80 mg, 0.23 mmol) in CH_2Cl_2 (5 mL) dropwise in an ice bath. The mixture was allowed to warm to room temperature and stirred for 24 h. Water was added while the reaction mixture was cooled in an ice bath. The mixture was extracted with $CHCl_3$ and the water layer was extracted with ethyl acetate. The organic phase was dried over Na_2SO_4 and filtered. The solvent was removed, and the residue was purified by silica gel chromatography (hexane/ethyl acetate = 4:1) to give 15 mg of **15** (19.5%). ^{1}H NMR (300 MHz, CD_3OD) δ 6.57 (s, 1H), 6.76 (d, J = 8.7 Hz, 2H), 7.16 (d, J = 8.7 Hz, 1H), 7.29 (dd, J = 1.5, 1.5 Hz, 1H), 7.60 (d, J = 8.7 Hz, 2H), 7.81 (s, 1H). HRMS m/z $C_{14}H_{10}NOI$ found 334.9808/calcd 334.9807 (M^+).

4.1.16. 2-(4-(5-Iodo-1*H*-indol-2-yl)phenoxy)ethanol (16)

A mixture of **15** (13 mg, 0.039 mmol), potassium carbonate (48 mg, 0.12 mmol) and ethylene chlorohydrin (4 μL, 0.06 mmol) in anhydrous DMF (3 mL) was stirred under reflux for 10.5 h. After cooling to room temperature, water was added, and the reaction mixture was extracted with $CHCl_3$. The organic layer was separated, dried over Na_2SO_4 and evaporated. The resulting residue was purified by preparative TLC (hexane/ethyl acetate = 1:1) to give 3 mg of **16** (20.4%). ^{1}H NMR (300 MHz, CD_3OD) δ 3.89 (t, J = 9.6 Hz, 2H), 4.09 (t, J = 9.3 Hz, 2H), 6.62 (s, 1H), 7.02 (d, J = 8.7 Hz, 2H), 7.17 (d, J = 8.1 Hz, 1H), 7.30 (dd, J = 1.8, 1.5 Hz, 1H), 7.70 (d, J = 9.0 Hz, 2H), 7.82 (s, 1H), 11.0 (s, 1H). HRMS m/z $C_{16}H_{14}NO_2I$ found 379.0078/calcd 379.0069 (M^+).

4.1.17. 4-(5-Bromo-1*H*-indol-2-yl)phenol (17)

The same reaction as described above to prepare **15** was used, and 13 mg of **17** was obtained in a 13.0% yield from **13** (105 mg, 0.347 mmol). ^{1}H NMR (300 MHz, CD_3OD) δ 6.58 (s, 1H), 6.84 (d, J = 9.0 Hz, 2H), 7.11 (dd, J = 1.8, 1.5 Hz, 1H), 7.25 (d, J = 8.7 Hz, 1H), 7.60 (d, J = 9.0 Hz, 3H).

4.1.18. 2-(4-(5-Bromo-1*H*-indol-2-yl)phenoxy)ethanol (18)

The same reaction as described above to prepare **16** was used, and 1.8 mg of **18** was obtained in a 14.2% yield from **17** (11 mg, 0.038 mmol). ^{1}H NMR (300 MHz, CD_3OD) δ 3.89 (t, J = 8.7 Hz, 2H), 4.09 (t, J = 9.6 Hz, 2H), 6.64 (s, 1H), 7.02 (d, J = 8.7 Hz, 2H), 7.13 (dd, J = 1.5, 1.5 Hz, 1H), 7.26 (d, J = 8.7 Hz, 1H), 7.61 (s, 1H), 7.70 (d, J = 8.7 Hz, 2H).

4.1.19. 2-(4-(5-(Trimethylstannyl)-1*H*-indol-2-yl)phenoxy) ethanol) (19)

The same reaction as described above to prepare **4** was used, and 9 mg of **19** was obtained in a 89.8% yield from **18** (8 mg, 0.02 mmol). ^{1}H NMR (300 MHz, $CDCl_3$) δ 0.31 (s, 9H), 3.99 (t, J = 8.7 Hz, 2H), 4.14 (t, J = 9.3 Hz, 2H), 6.71 (d, J = 11.1 Hz, 1H), 6.76 (d, J = 9.3 Hz, 1H), 6.98–7.08 (m, 2H), 7.39 (s, 1H), 7.57–7.62 (m, 2H), 7.88 (d, J = 9.3 Hz, 1H), 8.25 (s, 1H).

4.1.20. 4-(5-Bromo-1*H*-indol-1-yl)-*N*,*N*-dimethylbenzenamine (20)

A mixture of 5-bromoindole (100 mg, 0.51 mmol), 4-(dimethylamino)-phenylboronic acid (84 mg, 0.51 mmol), $Cu(OAc)_2$ (200 mg, 1.00 mmol), triethylamine (0.18 mL), and powdered molecular sieves 3 Å was suspended in CH_2Cl_2 (10 mL), and stirred for 1 h. The solvent was removed, and the residue was purified by silica gel chromatography (hexane/ethyl acetate = 9:1) to give 71 mg of **20** (44.2%). ^{1}H NMR (300 MHz, $CDCl_3$) δ 3.02 (s, 6H), 6.55 (d, J = 2.7 Hz, 1H), 6.82 (d, J = 9.0 Hz, 2H), 7.28 (d, J = 1.8 Hz, 1H) 7.78 (d, J = 1.2 Hz, 1H).

4.1.21. 4-(5-(Tributylstannyl)-1*H*-indol-1-yl)-*N*,*N*-dimethylbenzenamine (21)

The same reaction as described above to prepare **9** was used, and 21 mg of **21** was obtained in a 12.4% yield from **20** (102 mg, 0.32 mmol). ^{1}H NMR (300 MHz, $CDCl_3$) δ 0.87–1.56 (m, 27H), 3.02 (s, 6H), 6.61 (d, J = 3.3 Hz, 1H), 6.82 (d, J = 9.0 Hz, 2H), 7.24 (d, J = 3.0 Hz, 2H), 7.34 (d, J = 8.7 Hz, 2H), 7.45 (d, J = 3.0 Hz, 1H), 7.77 (s, 1H).

4.1.22. 4-(5-Iodo-1*H*-indol-1-yl)-*N*,*N*-dimethylbenzenamine (22)

The same reaction as described above to prepare **5** was used, and 8 mg of **22** was obtained in a 55.3% yield from **21** (21 mg, 0.04 mmol). ^{1}H NMR (300 MHz, $CDCl_3$) δ 3.02 (s, 6H), 6.54 (d, J = 3.3 Hz, 1H), 6.81 (d, J = 6.6 Hz, 2H), 7.20 (d, J = 7.8 Hz, 2H), 7.29 (d, J = 9.0 Hz, 2H), 7.41 (dd, J = 1.5, 1.8 Hz, 1H), 7.99 (d, J = 1.2 Hz, 1H). HRMS m/z $C_{16}H_{15}N_2I$ found 362.0287/calcd 362.0280 (M^+).

4.2. Iododestannylation reaction

The radioiodinated forms of compounds **5**, **11**, **14**, and **16** were prepared from the corresponding trimethyltin derivatives by iododestannylation using the previously described *N*-chlorosuccinimide (NCS) method, with some modifications.[26] Briefly, a 80 μL solution of **5**, **11**, **14**, and **16** in methanol containing 1% acetic acid (0.56 mg/mL) was mixed with 20 μL of NCS in methanol (0.5 mg/mL) in a sealed vial, and [^{125}I]NaI (0.1–0.2 mCi, specific activity 2200 Ci/mmol) was added. The reaction was allowed to proceed at room temperature for 20 s and terminated by addition of $NaHSO_3$. After extraction with ethyl acetate, the extract was dried by passing through an anhydrous Na_2SO_4 column and blown dry with a stream of nitrogen gas. The radioiodinated ligand was purified by HPLC on a Cosmosil C_{18} column with an isocratic solvent of H_2O/acetonitrile (4:6–1:1) at a flow rate of 1.0 mL/min.

4.3. Binding assays using the aggregated Aβ peptide in solution

A solid form of Aβ42 was purchased from Peptide Institute (Osaka, Japan). Aggregation was carried out by gently dissolving the peptide (0.25 mg/mL) in a buffer solution (pH 7.4) containing 10 mM sodium phosphate and 1 mM EDTA. The solution was incubated at 37 °C for 42 h with gentle and constant shaking. Binding assays were carried out as described previously.[27] [^{125}I]IMPY (6-iodo-2-(4′-dimethylamino)phenyl-imidazo[1,2]pyridine) with 2200 Ci/mmol specific activity and greater than 95% radiochemical purity was prepared using the standard iododestannylation reaction as described previously.[15] Binding assays were carried out in 12 × 75 mm borosilicate glass tubes. A mixture containing 50 μL of test compound (0.2 pM–400 nM in 10% EtOH), 50 μL of [^{125}I]IMPY (0.02 nM diluted in 50% EtOH), 50 μL of Aβ42 aggregates, and 850 μL of 10% ethanol was incubated at room temperature for 3 h. The mixture was then filtered through Whatman GF/B filters using a Brandel M-24 cell harvester, and the filters containing the bound ^{125}I ligand were placed in a gamma counter (Aloka, ARC-380). Values for the half-maximal inhibitory concentration (IC_{50}) were determined from displacement curves of three independent experiments using GraphPad Prism 4.0, and those for the inhibition constant (K_i) were calculated using the Cheng–Prusoff equation.[28]

4.4. Neuropathological staining of mouse brain sections

The experiments with animals were conducted in accordance with our institutional guidelines and approved by the Nagasaki University Animal Care Committee. *Tg2576* transgenic mice (female, 28 months old) and wild-type mice (female, 22 months old) were used as the Alzheimer's model and control, respectively. After the mice were sacrificed by decapitation, the brain was immediately removed and frozen in powdered dry ice. The frozen blocks were sliced into serial sections, 10 μm thick. Each slide was incubated with a 50% EtOH solution (100 μM) of compounds **11** and **14** for 10 min. The sections were washed in 50% EtOH for 1 min two times, and examined using a microscope (KEYENCE BZ-8100) equipped with a DAPI-BP filter set (excitation, 360 nm; diachromic mirror, 400 nm; longpass filter, 460 nm). Thereafter, the sections were also stained with thioflavin S, a pathological dye commonly used for staining Aβ plaques in the brain, and examined using a microscope (KEYENCE BZ-8100) equipped with a GFP-BP filter set (excitation, 470 nm; diachromic mirror, 495 nm; longpass filter, 535 nm).